

Effects of *Bacillus* sp. adhesion on cavitation erosion behaviour of nickel aluminium bronze in artificial seawater

Ye Tian^{a,b,1}, Hang Zhao^{a,b,1}, Rui Yang^{a,b,1}, Xiaomei Liu^{a,b}, Hua Li^{a,b}, Xiuyong Chen^{a,b,c,*}

^a Key Laboratory of Marine Materials and Related Technologies, Zhejiang Key Laboratory of Marine Materials and Protective Technologies, Ningbo Institute of Materials Technology and Engineering, Chinese Academy of Sciences, Ningbo, 315201, China

^b Zhejiang Engineering Research Center for Biomedical Materials, Cixi Institute of Biomedical Engineering, Ningbo Institute of Materials Technology and Engineering, Chinese Academy of Sciences, Ningbo, 315201, China

^c School of Engineering Science, University of Chinese Academy of Sciences, Beijing, 100049, China

ARTICLE INFO

Keywords:

Cavitation erosion
Bioadhesion
Microbiological corrosion
Nickel aluminium bronze
Failure mechanism

ABSTRACT

This study evaluated the cavitation erosion behaviour of a commonly used material in the marine environment, nickel aluminium bronze (NAB), after exposure to the adhesion of *Bacillus* sp. biofilm in artificial seawater. Results showed that the biofilm could inhibit the corrosion progress, keeping κ phases intact and subsequently allowing the NAB to retain its cavitation erosion resistance. Detailed discussion about the effect of the biofilm on cavitation erosion behaviour of NAB was presented. Furthermore, the importance of the κ phases for resisting cavitation erosion was evidenced by *in-situ* SEM, and a correlation of the decrease in hardness and the increase in mass loss during cavitation erosion was built.

1. Introduction

For a vessel travelling from the river to the shore, its propeller and rudder are exposed to cavitation erosion and subsequently cavitation erosion-corrosion, as the schematic illustration shown in Fig. 1. Cavitation erosion frequently occurs to ship propellers causing severe wear [1,2]. When a propeller is operated at high speed, the pressure fluctuation of the surrounding water results in the formation of cavitation bubbles. Microjets are generated when cavitation bubbles collapse, of which the velocity can reach up to 4000 m/s [3]. The impact load of the microjet on the propellers usually ranges from 0.2 to 2 GPa, while some can even reach 10 GPa [4], resulting in severe wear on the surface of a propeller and a significant reduction of its service time. In addition, as operated in seawater, corrosion is also a critical issue, and the synergistic effect of cavitation erosion-corrosion can further accelerate the material wear [2,5].

When the vessel further travels in the ocean, biofouling is another typical damage to the propeller. In the marine environment, biofouling caused by bacterial adhesion significantly affects the corrosion of materials. There are two types of influence of bacterial adhesion on the corrosion of materials, namely microbiologically influenced corrosion

(MIC) and microbiologically influenced corrosion inhibition (MICI) [6]. Sheng et al. [7] explored the effect of the attachment of sulfate-reducing bacteria *Desulfovibrio desulfuricans* on the corrosion resistance of 316 stainless steel. The results showed that with the sulfate as the electron acceptor and reduced to sulfide (Such as H₂S & FeS), biofilm accelerated the corrosion rate of 316 stainless steel. Xu et al. [8] studied the effect of the attachment of nitrate-reducing bacteria *Bacillus licheniformis* on C1018 carbon steel. The study found the formation of iron nitride (such as FeN, Fe₃N, and Fe₄N) on the surface, indicating the attachment of biofilm promoted the electron transfer of iron (Fe⁰) to nitrogen (N₂), which may lead to severe corrosion. Similar MIC results have also been discovered in previous studies [9–13]. However, bacterial attachment may also inhibit the corrosion rate of materials (MICI effect). Li et al. [14] investigated the effect of *Bacillus cereus* attachment on the corrosion behaviour of 316 stainless steel and found that the biofilm of *Bacillus cereus* enhanced the corrosion resistance via blocking the electron transfer between the steel and the cathodic depolarizer. Other studies indicated that the bioadhesion of some particular microorganisms on certain materials may significantly reduce the corrosion current, which could be attributed to the microorganisms-induced changes of the type and concentration of ions, oxygen level, and pH on the surface of the

* Corresponding author. Key Laboratory of Marine Materials and Related Technologies, Zhejiang Key Laboratory of Marine Materials and Protective Technologies, Ningbo Institute of Materials Technology and Engineering, Chinese Academy of Sciences, Ningbo, 315201, China.

E-mail address: chenxiuyong@nimte.ac.cn (X. Chen).

¹ These authors contributed equally: Ye Tian, Hang Zhao, Rui Yang.

<https://doi.org/10.1016/j.wear.2022.204344>

Received 31 December 2021; Received in revised form 16 March 2022; Accepted 4 April 2022

Available online 6 April 2022

0043-1648/© 2022 Elsevier B.V. All rights reserved.

coating [15–19].

Nickel aluminium bronze (NAB), as one of the most common propeller materials, has been extensively studied on its cavitation erosion and corrosion behaviours for several decades. Meanwhile, the cavitation erosion-corrosion synergy in related to the microstructure of NAB also has been widely investigated recently [20–23]. Some literature used in-situ electrochemical corrosion test to further reveal the synergism effect of cavitation erosion and corrosion [24,25]. Despite the extensive studies on the synergies of the bioadhesion-corrosion and the cavitation erosion-corrosion, the effect of bioadhesion on cavitation erosion-corrosion has not been reported yet (Fig. 1). Since bioadhesion may have different effects on corrosion and corrosion usually accelerates material wear when the material is exposed to cavitation erosion, it is worthwhile to investigate the effects of bioadhesion on cavitation performance of materials. Therefore, this study aims to investigate the effect of *Bacillus* sp. adhesion on cavitation erosion of NAB in artificial seawater (ASW), intending to gain insight into the connection of biofouling and cavitation erosion-corrosion.

2. Experimental

2.1. Materials

Commercially available cast NAB (Suzhou Zhongmai Copper Ltd., China) was used. The dimension of the cylindrical NAB samples was $\Phi 20 \times 10$ mm, and the composition was tabulated in Table 1. Before testing, the top surface of the NAB samples was ground with 800-mesh sandpaper and then polished with a diamond (1 μm) suspension (Wuyi Hengyu Instrument Ltd., China). Regents (all the reagents were supplied by Sinopharm Chemical Reagent Ltd., China in this work, unless specified) were used to prepare an etching solution and ASW. The etching solution for NAB was composed of FeCl_3 (solid, 5 g) and HCl (37 wt% in aqueous solution, 2 ml) in 95 mL of ethanol, and the etching time was 3 s for the characterisation of the polished NAB samples [26]. The preparation of the ASW was as per ASTM D1141-98 (2003) [27]. In addition, bacteria contained ASW (BASW) was also prepared. The culture medium was composed of peptone (3 g/L) in ASW and autoclaved at 121 $^\circ\text{C}$ for 20 min before the inoculation of *Bacillus* sp. (MCCC1A00791, Marine Culture Collection of China, China).

2.2. Corrosion in ASW

The NAB samples were sealed with epoxy resin except for the polished surface. Then, the partially sealed samples were immersed into a beaker containing 2 L of ASW for 7, 15, 30, and 60 days, respectively. The ASW in the beaker was refreshed every 7 days and kept at a constant

temperature of 28 ± 2 $^\circ\text{C}$. Next, the samples were cleaned with deionised water for 5 min and subsequently with nitric acid (17 wt% in aqueous solution) for 2 min in an ultrasonic bath to remove the corrosion products [28] for scanning electron microscopy (SEM, Regulus 8230, Hitachi High-Tech Ltd., Japan) and cavitation erosion. The corrosion products from the sample immersed in ASW for 30 days were collected, cleaned, and dried for X-ray diffraction (XRD, D8 Advance, Bruker Instruments Ltd., USA) using a copper anode at 40 kV and 40 mA.

2.3. Bioadhesion of *Bacillus* sp. and corrosion in BASW

The partially sealed NAB samples were immersed in BASW (10^6 bacteria/ml on day 0) at 28 ± 2 $^\circ\text{C}$. Every 2 days, 67% of the BASW was replaced by an autoclaved culture medium to maintain the normal growth of bacteria. The samples were taken out on the 7th, 15th, 30th, and 60th days to observe the surface morphologies after bacterial attachment. Some bacteria adhered NAB samples were immersed in 2.5% glutaraldehyde at 4 $^\circ\text{C}$ for 2 h and then consecutively dehydrated in 25, 50, 75, 90, and 100 vol% (twice in 100 vol%) ethanol solutions for the SEM observation of the biofilm on the samples. In addition, the composition of the biofilm on the samples immersed in BASW for 30 days was investigated by Fourier transform infrared spectroscopy (FT-IR, Nicolet 6700, Thermo Fisher Scientific Ltd., USA). The others were immersed in an ultrasonic bath with deionised water for 5 min and subsequently with nitric acid (17 wt% in aqueous solution) for 2 min to remove the biofilm and corrosion products [28] for SEM characterisation and cavitation erosion.

2.4. Electrochemical measurements

Electrochemical tests (CHI660E electrochemical workstation, Shanghai Chenhua Instrument Ltd., China) were carried out to acquire the Nyquist plots and Tafel curves of the samples after 30 days of immersion in the ASW/BASW solutions. A typical three-electrode system was adopted, where a saturated calomel electrode and a platinum foil were used as the reference and the counter electrodes, respectively. The Nyquist plots were measured by a sinusoidal potential disturbance with the amplitude of 5 mV in the frequency range of 10^5 to 10^{-2} Hz. Meanwhile, the Tafel curves were conducted at the rate of 5×10^{-4} V/s from -1.0 to 0 V. The Nyquist plots and the Tafel curves were conducted in the ASW medium at 25 ± 1 $^\circ\text{C}$ and repeated 3 times to ensure reproducibility.

2.5. Vickers hardness test

Vickers hardness test (Wilson VH3300, Buehler Ltd, Germany) was

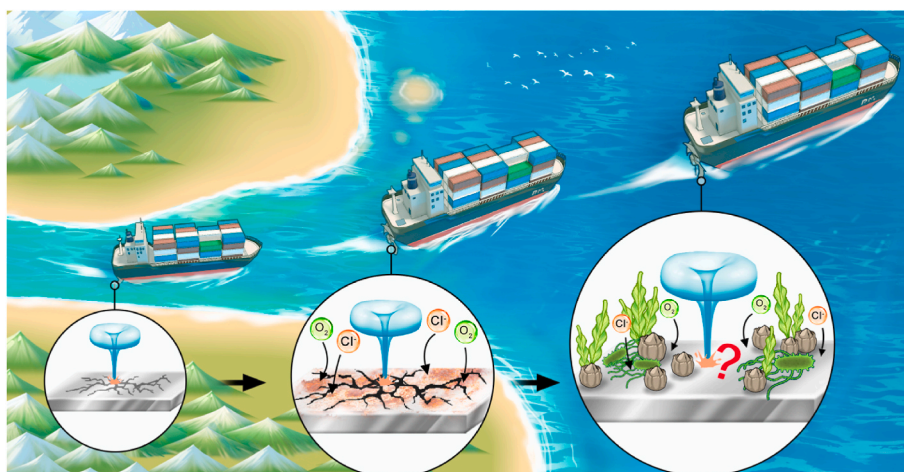


Fig. 1. The effect of biofouling on the cavitation erosion-corrosion was unrevealed.

Table 1
Composition of cast nickel aluminium bronze alloy.

Elements	Ni	Al	Fe	Mn	Si	C	Cu
wt.%	4.0–5.0	8.5–10.0	4.0–5.0	0.8–2.5	<0.15	<0.10	bal.

performed on the NAB samples immersed in ASW and BASW for 0, 7, 15, 30, and 60 days. Before testing, the corrosion products and biofilm were removed. For each sample, five random locations in the surface were indented under a load of 10 kgf with a dwell time of 10 s, and the average value and the standard deviation of the Vickers hardness were calculated.

2.6. Cavitation erosion-corrosion

The cavitation erosion test was performed in ASW using ultrasonic vibration apparatus (GBS-SCL 15K, Hangzhou Guobiao Ultrasonic Equipment Co., Ltd., Zhejiang, China) as per a modified version of ASTM G32-16 [29] on the polished, the ASW-immersed, and the BASW-immersed NAB samples (the corrosion products and the biofilms were removed before the test). A schematic diagram of the apparatus for the test is shown in Fig. 2 [30]. The apparatus was operated at a frequency of 20 kHz with a peak-to-peak amplitude of 50 μm . The horn was immersed at a depth of 23 ± 2 mm in the test medium, which was kept at 25 ± 2 °C by a cooling system. The sample was fixed coaxially with the horn at 1 mm to the horn tip.

For the ASW/BASW-immersed NAB samples exposed to cavitation erosion in ASW, both types of the samples entered the steady-state period after 6 h, at which the mass loss rate was stable. Therefore, the cumulative mass loss of the samples exposed to 6 h of cavitation erosion was used to evaluate the cavitation erosion performance of the samples. Before and after 6-h cavitation erosion, the samples were rinsed, dried, and weighed to calculate mass loss (accurate to 0.1 mg). The cavitation erosion test was repeated three times for each group of the sample to get the average value and the standard deviation. Furthermore, *in-situ* SEM observation was undertaken to study the cavitation erosion-corrosion failure mechanism of the NAB. Specifically, the surface morphology at the same position of the polished NAB sample was observed by SEM before (0 min) and after cavitation erosion-corrosion at the 40th, 100th, and 160th mins.

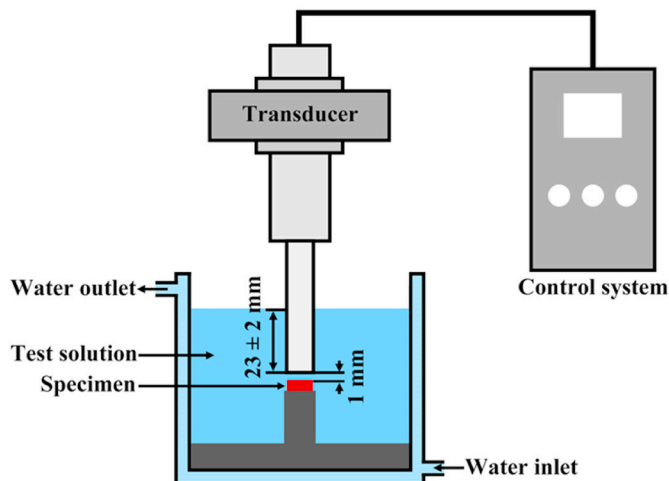


Fig. 2. Schematic diagram of the cavitation erosion test apparatus.

3. Results and discussion

3.1. Microstructure and cavitation erosion behaviour of original NAB

The etched NAB shows its microstructure consists of α phase (fcc copper-rich) and the β' phase (or retained β phase) (Fig. 3a), which were surrounded by a variety of intermetallic κ -phases (κ_I , κ_{II} , κ_{III} , and κ_{IV}) (Fig. 3b) [31–33]. The κ_I phase has a rosette-like morphology and its main composition was Fe_3Al , which could be observed within the α phase matrix [31]. The κ_{II} phase also presented a rosette-like morphology and was smaller than the κ_I phase [33]. The nickel-rich (based on NiAl) κ_{III} phase can be found at the boundary of the large κ_I phase or at the α - β' boundaries [34]. The κ_{IV} phase is an iron-rich precipitate that appeared within the α phase, of which the size is very small [35].

The cavitation erosion behaviour of the polished NAB sample was revealed by *in-situ* SEM observation Fig. 4. Before cavitation erosion (Fig. 4a), the κ_{II} , κ_{III} , and κ_{IV} phases (highlighted by the red dotted circle, black arrow, and blue arrow, respectively) were tightly bonded to the surrounding α phase matrix without any crack. As exposed to cavitation erosion for 40 min (Fig. 4b), cracks were observed near the boundaries of the κ and α phases. After 100 min of cavitation erosion (Fig. 4c), a large cavitation crater was formed due to the detachment of the κ_{II} phase. Meanwhile, small cavitation craters also appeared as the removal of κ_{III} and κ_{IV} phases. These cavitation craters got expanded when further exposed to cavitation erosion (Fig. 4d), as the exposed α phase matrix could be easily peeled off from the NAB without the protection by the hard κ phases. The results from the *in-situ* SEM observation of the NAB exposed to cavitation erosion in ASW suggested that the κ phases were of great importance for NAB to resist cavitation erosion. Specifically, κ phases exhibited high hardness, and the dispersion of the hard κ phases in NAB provided good cavitation erosion resistance. When the κ phases were detached, the remained α phase could not resist cavitation erosion effectively. Meanwhile, cracks could be introduced during the detachment of κ phases, resulting in the accelerated removal of the α phase. Furthermore, when NAB was immersed in ASW for a long time or used in other complex environments with microorganisms, corrosion and bioadhesion can also change the microstructure evolution of the κ phases and thus affect the cavitation erosion behaviours of the NAB. Therefore, it is worthwhile to investigate the effect of long-term exposure to the ASW and BASW on the microstructure of the NAB, which can assist the understanding of the cavitation erosion behaviours in turn.

3.2. Microstructure, corrosion behaviour, and microhardness of the NAB exposed to corrosion and bioadhesion

The surface morphologies of the NAB samples after immersion in BASW is shown in Fig. 5. Only a few bacteria were observed on the surface of the sample after immersion for 7 days (Fig. 5a). Then, the number of bacteria increased significantly with the prolongation of immersion (Fig. 5b and c). Finally, the sample was entirely covered by a homogeneous biofilm after 60 days of immersion (Fig. 5d). The sample immersed in BASW for 30 days was further characterised by FT-IR (Fig. 6). The absorption peak at ~ 3420 cm^{-1} could be attributed to the O–H stretching vibration, and the O–H bond was the functional group of proteins and polysaccharides [36]. The absorption peak at ~ 1020 cm^{-1} was caused by CO– stretching in ribose and glycopeptides [28]. The absorption peak at ~ 1660 cm^{-1} referred to C–N (Amide I) and C=O stretching, and the absorption peak at ~ 1540 cm^{-1} was resulted from the NH bending and C–N (Amide II) stretching. The Amide I and

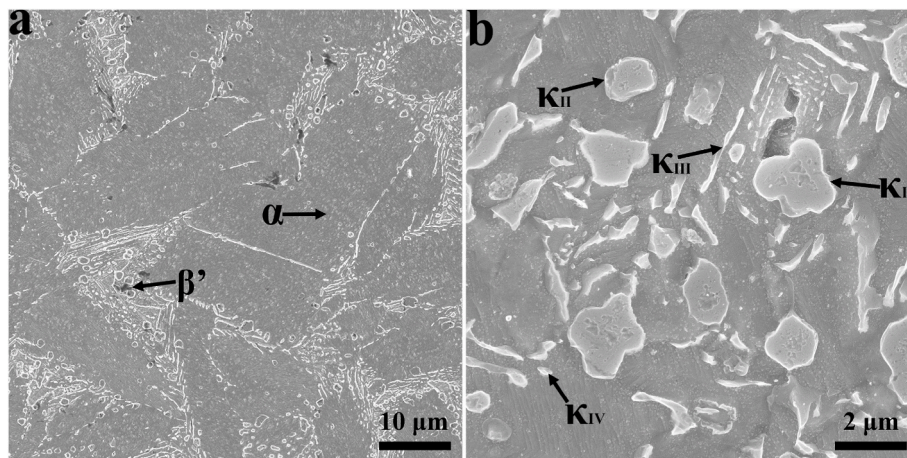


Fig. 3. Microstructure of the original NAB. a, low magnification; b, high magnification.

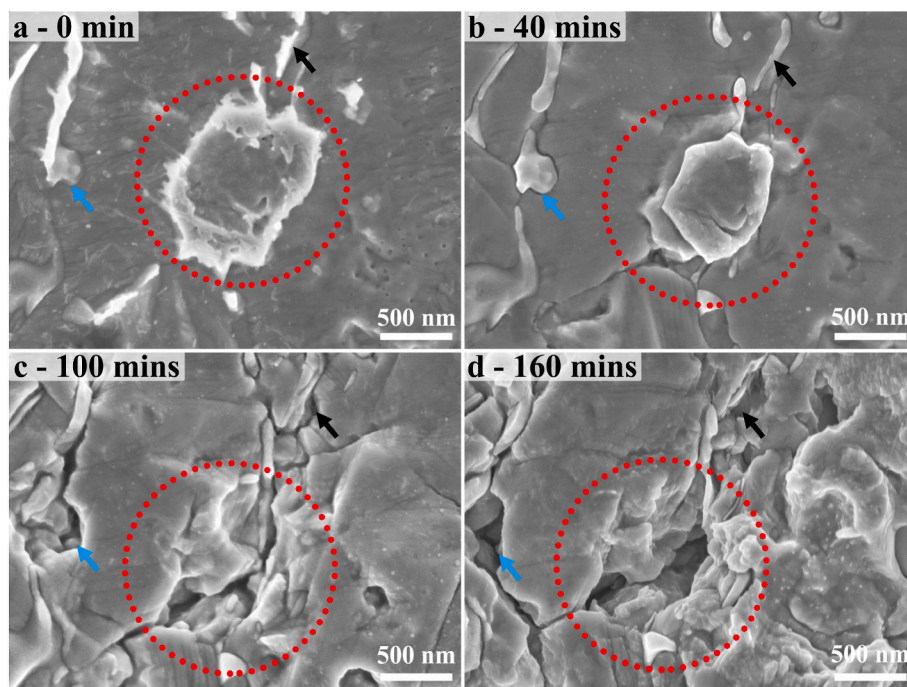


Fig. 4. Microstructure evolution of the original NAB exposed to cavitation erosion in ASW. a, as-polished surface; b–d, surface subjected to cavitation erosion in ASW for 40, 100, 160 min, respectively; Interested regions: κ_{II} phase (red dotted circle), κ_{III} phase (black arrow), and κ_{IV} phase (blue arrow). (For interpretation of the references to colour in this figure legend, the reader is referred to the Web version of this article.)

Amide II were the functional groups of proteins [37,38]. Therefore, the colonisation of the *Bacillus* sp. and the formation of the biofilm was evidenced by these structural features confirmed by the FT-IR result (Fig. 6).

Biofilm can significantly affect the corrosion rate of the materials, which eventually changes the surface morphologies of the samples. The comparison for the surface morphologies of the NAB samples exposed to corrosion and bioadhesion after cleaning out the corrosion products and biofilm is demonstrated in Fig. 7. As shown in Fig. 7a1, some small corrosion pits appeared on the surface after 7 days of immersion in ASW. The width of the corrosion pit grew larger as the immersion time extended (Fig. 7b1–c1). On the 60th day of immersion in ASW (Fig. 7d1), the surface was severely damaged, and a considerable amount of α phase was dissolved into the ASW [39,40], resulting in the formation of large craters. However, for the NAB sample immersed in BASW (Fig. 7a2–d2), only some small cracks were observed on the surface after 60 days of

immersion (Fig. 7d–2), different from the sample immersed in ASW. Thus, it is concluded that the biofilm (by *Bacillus* sp.) can inhibit the corrosion of NAB in ASW, possibly via blocking the extracellular electron transfer and thereby suppressing the process of metal dissolution [14].

The cross-sectional morphologies of the NAB samples after immersion in ASW and BASW also demonstrated the differences in the corroded morphologies of the NAB with and without the *Bacillus* sp. biofilm adhesion Fig. 8. Generally, the surface of the NAB samples immersed in BASW was less rough than that immersed in ASW. Furthermore, the pits in the ASW-immersed samples tended to expand on the surface and grow into the surface (Fig. 8a and b), while the pits in the BASW-immersed samples only got expended in surface (Fig. 8c and d). Such differences in the growth of corrosion pit could be attributed to the fact that the biofilm could inhibit the dissolution of elements from the surface of the samples immersed in BASW [14]. In addition, for the

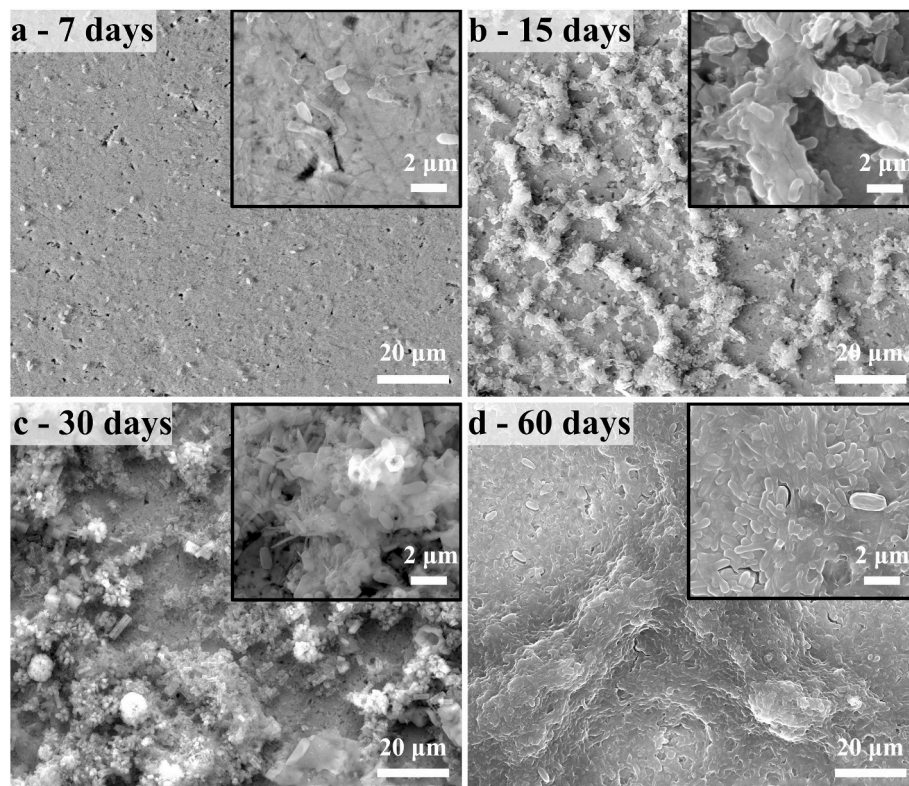


Fig. 5. Surface of the NAB samples after the immersion in BASW. a-d, at the 7th, 15th, 30th, and 60th days of immersion, respectively.

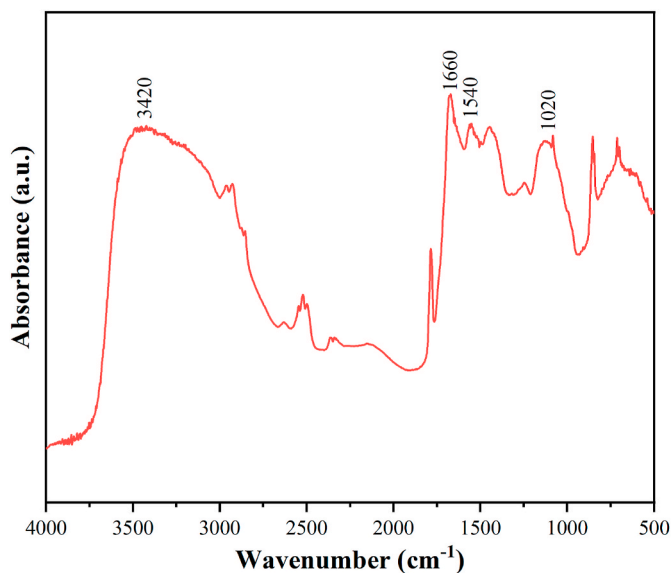


Fig. 6. FT-IR spectrum of the biofilm from the samples immersed in BASW for 30 days.

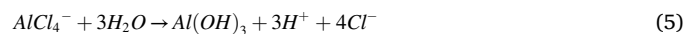
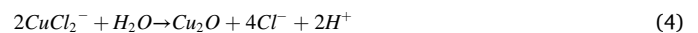
NAB immersed in ASW, the formation of the corrosion products film could bring negative impact to the corrosion resistance due to its porous and loose structure [41–43].

The characterisation of the chemical composition of the corrosion product assists the investigation of the corrosion process. Therefore, the corrosion products of the NAB in ASW was examined by XRD (Fig. 9), showing a composition of $\text{Cu}_2(\text{OH})_3\text{Cl}$, Al_2O_3 , and $\text{Cu}(\text{OH})_2$. Here, a possible route for the formation of the corrosion products was deduced according to the XRD result and the literature. The corrosion products were formed with the dissolution of Cu and Al from NAB in ASW in the

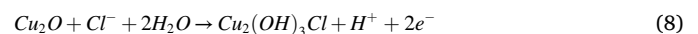
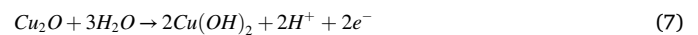
following process [40,43–46]:



As the CuCl_2^- and AlCl_4^- are unstable, Cu_2O and Al_2O_3 were formed subsequently through the following reaction [47–49]:



With the extended exposure time, the Cu_2O could be further oxidized to $\text{Cu}(\text{OH})_2$ and $\text{Cu}_2(\text{OH})_3\text{Cl}$ according to equations (7) and (8) [41,42]:



The Al_2O_3 can improve the corrosion resistance of NAB, whereas the porous of the $\text{Cu}(\text{OH})_2$ and the loose structure of the $\text{Cu}_2(\text{OH})_3\text{Cl}$ can negatively affect the corrosion resistance of NAB [21,41,42]. Generally, the potential difference between different phases (α , β' , and $\kappa_{\text{I-IV}}$) can be considered as the driving force for the selective phase corrosion of NAB [39]. The Al-rich κ -phases ($\kappa_{\text{I-IV}}$) present relatively higher nobility due to the formation of an Al_2O_3 protective film in the corrosive solution [50]. As a result, the copper-rich α - and β' -phases become anodic to the κ -phases and are preferentially corroded in the corrosive medium (Fig. 7) [51].

Electrochemical analyses were conducted to further reveal the effect of the biofilm on corrosion damage. The Tafel curves of the samples after 30 days of immersion in the ASW/BASW solutions are shown in Fig. 10. Meanwhile, the fitting results of the Tafel curves are tabulated in

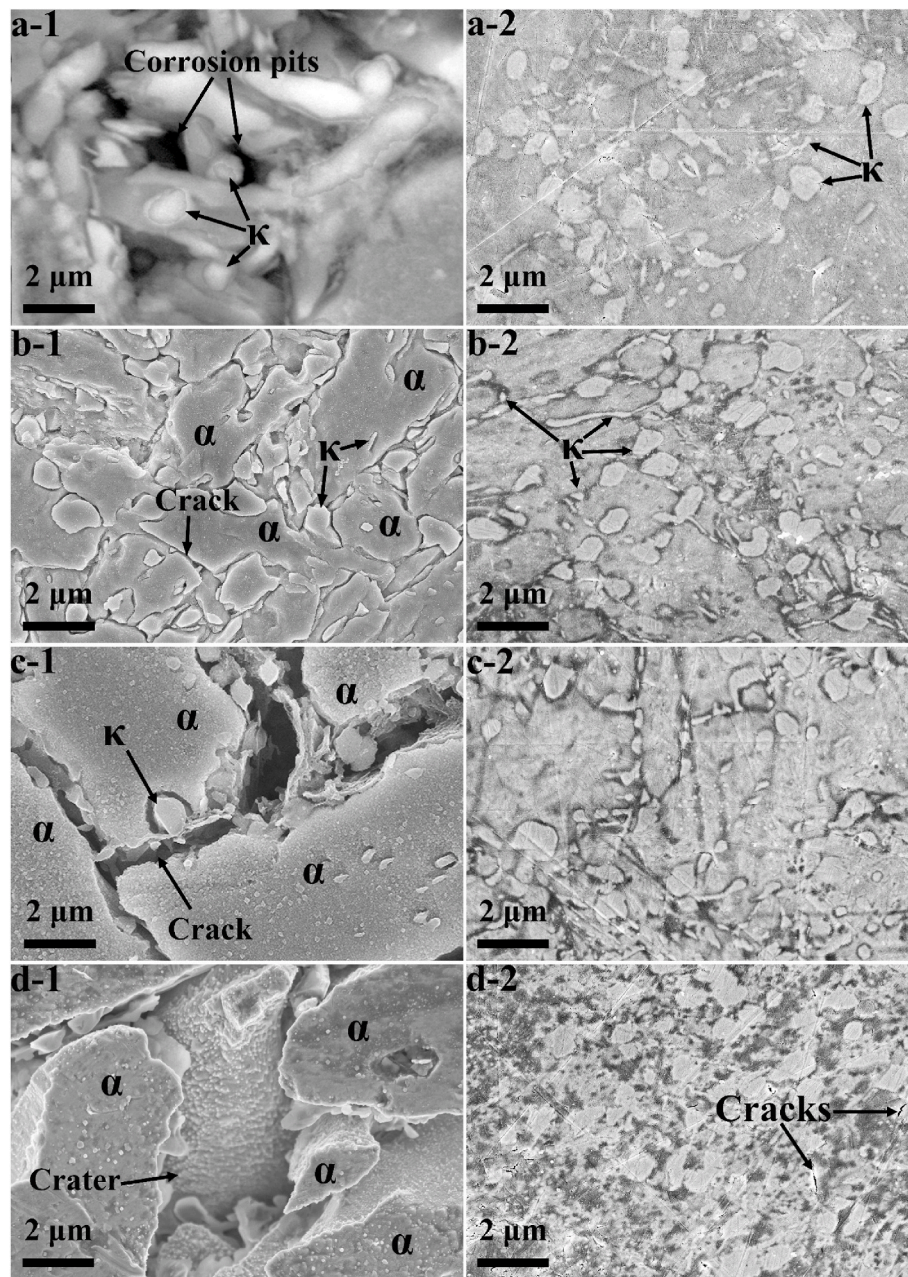


Fig. 7. Surface of the NAB samples. –1, after immersion in ASW; –2, after immersion in BASW; a–d, at the 7th, 15th, 30th, and 60th days of immersion, respectively. The corrosion products and the biofilm have been removed before observation.

Table 2, showing the corrosion potential (E_{corr}) and the corrosion current (I_{corr}) of the ASW-/BASW-immersed samples. According to Table 2, the E_{corr} and the I_{corr} of the BASW-immersed sample are higher and lower than the ASW-immersed sample, respectively. For the samples evaluated in the same test condition, a high E_{corr} and a low I_{corr} suggest a low corrosion rate [52]. Hence, the results from the Tafel curves are in agreement with the surface morphologies (Fig. 7). The difference in the corrosion resistance of the two samples is possibly due to the different barrier properties of the surface films (corrosion product film and bacterial biofilm) to the corrosive ions.

The barrier properties (corrosion product film and bacterial biofilm) of the ASW-immersed and the BASW-immersed samples were evaluated via electrochemical impedance spectroscopy (EIS) in the ASW solution. The Nyquist plot based on the data from the EIS results (fitted by Zsimpwin software) is presented in Fig. 11a. The radius of the semicircle in the Nyquist plot of the BASW-immersed sample is significantly larger

than that of the ASW-immersed sample. Generally, a large radius of the semicircle in a Nyquist plot indicates strong corrosion resistance [53]. To better understand the electrochemical processes during the ASW-/BASW immersion of the samples, equivalent circuit models (Fig. 11b) are built to simulate the EIS results, and the extracted results from the fit EIS data were tabulated in Table 3. After 30 days of immersion, the ASW-immersed sample matched model $R(Q(R(Q(RW))))$ well, while the BASW-immersed sample matched model $R(QR)(QR)$. As the corrosion resistance could be assessed by polarization resistance (R_p , $R_p = R_c + R_{ct}$) [53], the R_p values of the ASW-immersed and the BASW-immersed samples were calculated, which were 3474 ± 107 and $23827 \pm 930 \Omega \text{ cm}^2$, respectively. The significantly higher R_p values of the BASW-immersed sample indicates that the *Bacillus* sp. biofilm can effectively inhibit the corrosion of samples, which is in accordance with the surface morphologies (Fig. 7) and the Tafel curves (Fig. 10).

As the prolongation of immersion in ASW and BASW, the continuous

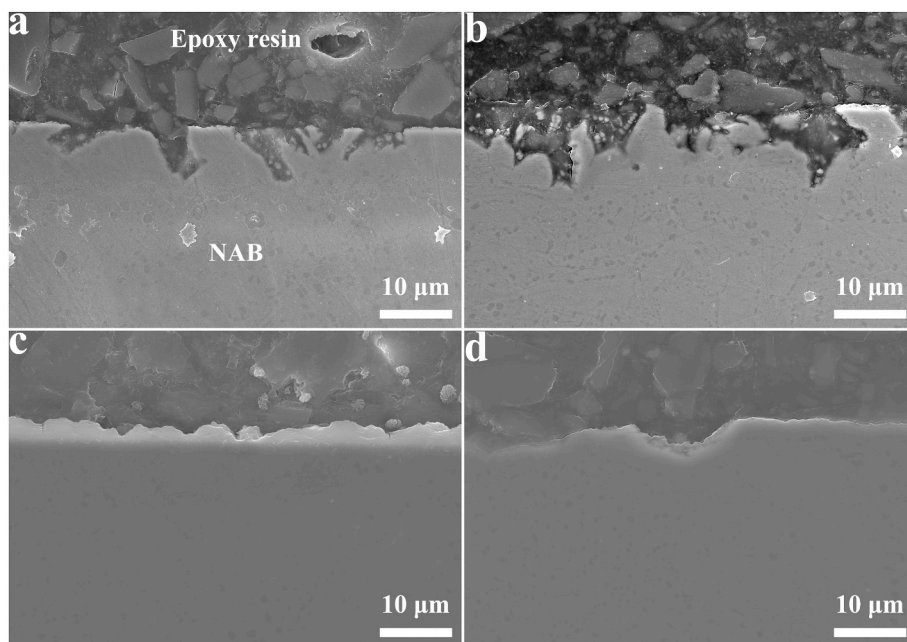


Fig. 8. Cross-section of the NAB samples. a-b, after immersion in ASW for 30 and 60 days, respectively; c-d, after immersion in BASW for 30 and 60 days, respectively. The corrosion products and the biofilm have been removed before observation.

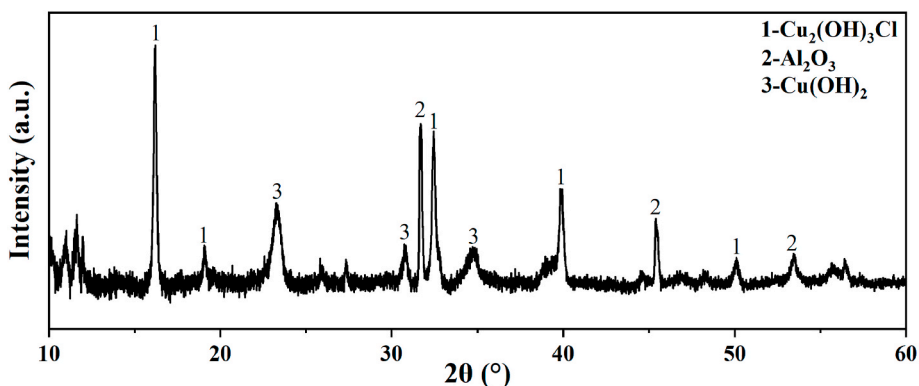


Fig. 9. XRD spectrum of the corrosion products of the NAB after 30 days of immersion in ASW.

dissolution of Cu and Al can cause the exposure and subsequently the peel-off of the κ phases, therefore reducing the hardness of the NAB (Fig. 12). The Vickers hardness (Hv_{10}) of NAB samples immersed in ASW and BASW continually decreased with the immersion time, while the decrease of the hardness of the sample immersed in BASW was much slower. The difference in the decrease of the hardness may be attributed to two explanations. Firstly, the corrosion products film of the NAB samples by the immersion in ASW could not prevent further corrosion, causing the continuous precipitation of copper at the grain boundary of the α phase. As the prolongation of immersion, numerous corrosion pits were formed at the grain boundaries of the α phase (Fig. 7b1-d1), which could reduce the hardness of the samples. However, protected by the biofilm, the grain boundary of the α phase of the samples immersed in BASW did not receive severe damage (Fig. 7a2-d2). Thus, the different severity of the damage in the α phase resulted in the difference in the hardness of the NAB samples immersed in ASW and BASW. Secondly, the κ phases performed high hardness with the function of dispersion strengthening in the NAB. The effect of phase-selective corrosion can cause severe damage in the α phase and then results in the exposure and the detachment of the κ phases on the surface of the ASW-immersed samples (Fig. 7a1-d1). However, even if the NAB sample was

immersed in BASW for 60 days (Fig. 7d2), limited κ phases on the surface were detached. As a result, the difference in the amount of the remained κ phases also caused different hardness of the NAB samples.

3.3. Effect of biofilm on cavitation erosion performance of NAB

Cavitation erosion performance of the ASW/BASW-immersed NAB samples was evaluated in ASW, and the cumulative mass loss of the samples exposed to 6 h of cavitation erosion was presented in Fig. 13. The cumulative mass loss of the samples immersed in ASW for 7 days was 9.7 mg, while that of the samples immersed for 60 days was 18.2 mg, showing an increased mass loss of 87.63%. However, such a large increment was not observed in BASW-immersed samples. The cumulative mass loss only increased from 8.2 mg (BASW immersion for 7 days) to 9.7 mg (BASW immersion for 60 days), presenting an increase of 18.29%. The differences (in percentage) in the cumulative mass of the ASW- and BASW-immersed samples for the same duration of immersion were also shown in Fig. 13. As the increased duration of immersion in ASW/BASW, the difference gradually became distinct (7 days: 18.56%, 15 days: 27.43%, and 30 days: 41.78%). At the 60th day immersion, the mass loss after cavitation erosion of the NAB samples immersed in BASW

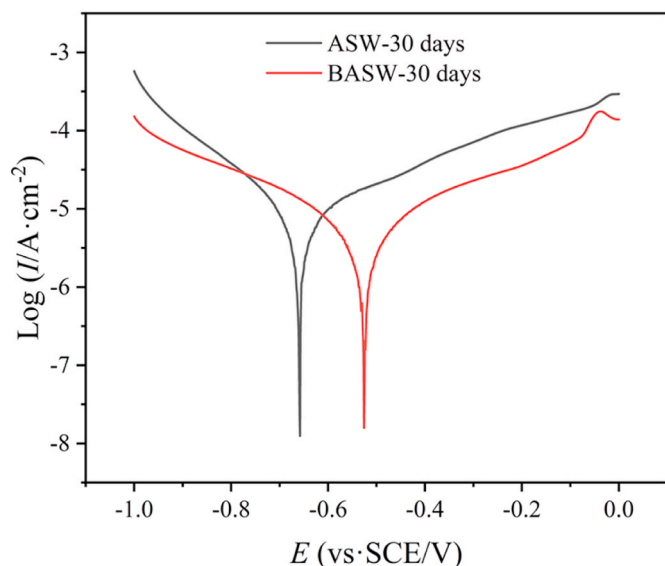


Fig. 10. Tafel curves of the samples after immersion in ASW/BASW for 30 days.

Table 2
Electrochemical parameters fitted from the Tafel curves.

Sample	E_{corr} (V)	I_{corr} ($\mu\text{A}\cdot\text{cm}^{-2}$)
ASW-immersed (30 days)	-0.66 ± 0.03	8.32 ± 0.15
BASW-immersed (30 days)	-0.53 ± 0.02	4.19 ± 0.08

was 46.70% lower than that of the samples immersed in ASW. At the beginning of immersion, the selective phase corrosion preferentially occurs in the copper-rich α and β' phases, resulting in the exposure of the κ -phases. After more immersion, the κ -phases were peeled off from the surface of the ASW-immersed samples, leading to the formation of corrosion pits and cracks (Fig. 7a1-b1) [40]. After a long-time immersion, large corrosion craters are formed due to the continuous dissolution of the α phases at the edge of the corrosion pits and cracks (Fig. 7c1-d1) [54]. Since the corrosion pits, cracks, and craters are the starting sites of cavitation erosion [30,55,56], severer cavitation erosion can happen if the number of these starting sites increases. For the BASW-immersed samples, only some cracks were observed even after 60 days of immersion (Fig. 7d2), and thus the BASW-immersed samples have a lower mass loss than the ASW-immersed samples in the cavitation

erosion tests. This result suggests that *Bacillus* sp. attachment can inhibit corrosion on the NAB sample surface, resulting in fewer starting sites of cavitation erosion and less cavitation mass loss.

As mechanical properties may be correlated to the cavitation erosion resistance, the correlation between the increased mass loss (I_M) and the decreased hardness (D_{Hv}) for the ASW/BASW-immersed NAB samples subjected to cavitation erosion for 6 h was investigated (Fig. 14). A

Table 3
Detailed electrochemical parameters of the samples after 30 days of immersion in ASW/BASW.

Parameters	ASW-30days	BASW-30days
R_s ($\Omega\cdot\text{cm}^2$)	6.30 ± 0.06	8.61 ± 0.05
Q_c (10^{-5} S·sec ⁿ ·cm ⁻²)	31.46 ± 1.92	3.44 ± 0.11
n_1	0.67 ± 0.01	0.60 ± 0.01
R_c ($\Omega\cdot\text{cm}^2$)	421 ± 7	21850 ± 776
Q_{dl} (10^{-5} S·sec ⁿ ·cm ⁻²)	11.28 ± 1.80	30.60 ± 0.80
n_2	0.86 ± 0.04	0.91 ± 0.02
R_{ct} ($\Omega\cdot\text{cm}^2$)	3053 ± 100	1977 ± 154
Z_w (10^{-3} s s ^{1/2} cm ⁻²)	2.35 ± 0.16	–
χ^2 (10^{-4})	7.53 ± 0.19	3.00 ± 0.15

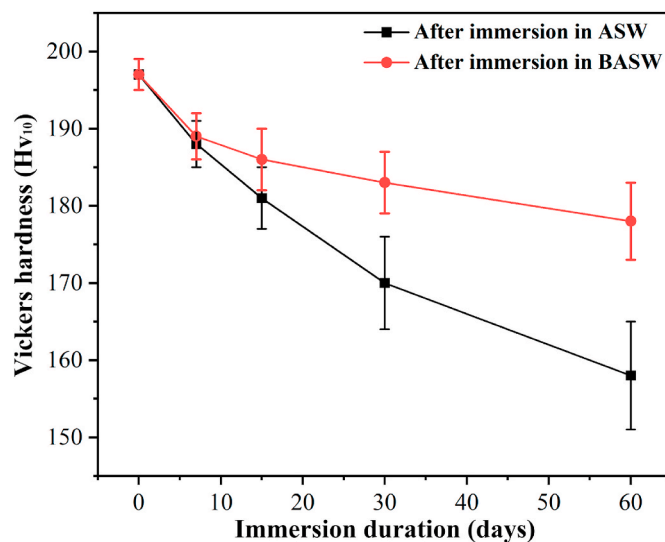


Fig. 12. Vickers hardness of the NAB samples after immersion in ASW and BASW. The durations of immersion were 0, 7, 15, 30, and 60 days.

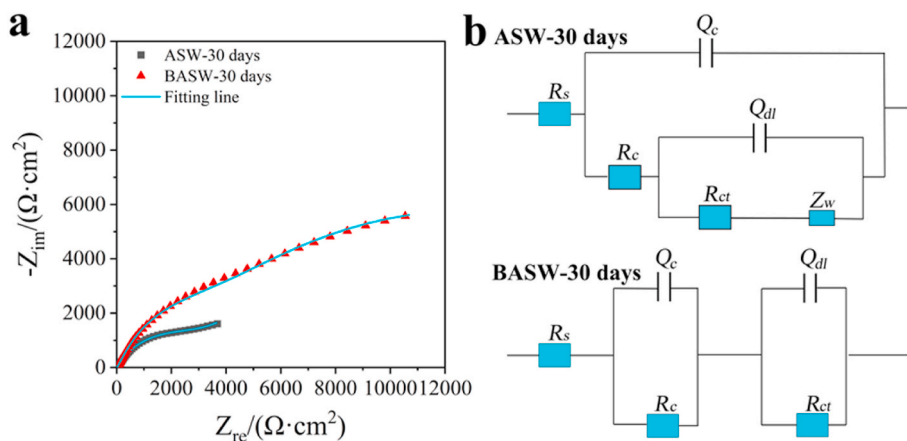


Fig. 11. Nyquist plots (a) and equivalent circuit models (b) for the samples after 30 days of immersion in ASW/BASW. R_s , R_c , Q_c , R_{ct} , Q_{dl} , and Z_w represent the solution resistance, corrosion product film/bacterial biofilm resistance, corrosion product film/bacterial biofilm constant phase, charge transfer resistance, double-layer constant phase, and finite-length diffusion of ions, respectively.

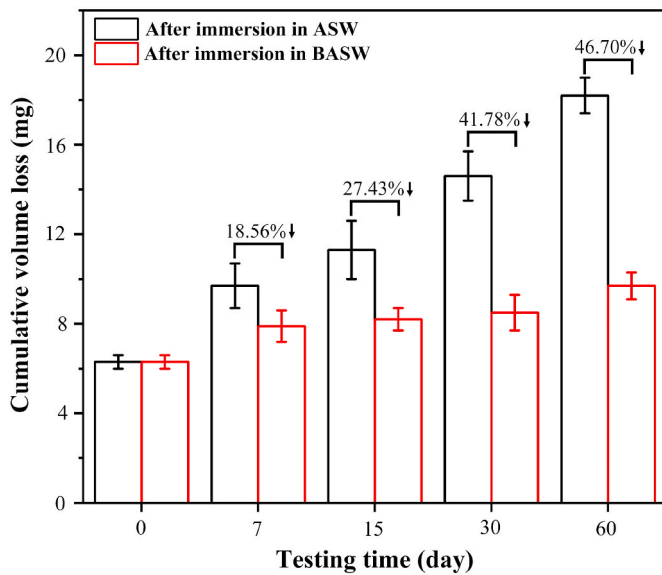


Fig. 13. The cumulative mass loss of the ASW/BASW-immersed NAB samples after 6 h of cavitation erosion in ASW.

linear relationship between D_{Hv} and I_m was drawn for the ASW-immersed samples (Fig. 14a), while the relationship was quadratic for the BASW-immersed samples (Fig. 14b). The functions are presented in Fig. 14, of which the coefficient of determination (R^2) was 0.998 and 0.996 for the ASW- and the BASW-immersed samples, respectively, evidencing the reliability of the fitting [57]. Other studies have also shown a significant correlation between the cavitation resistance and hardness of NAB alloys [22,26,58]. Furthermore, the fitting indicated that the cavitation erosion resistance of NAB was closely related to the hardness, and the hardness could be used to predict the cavitation erosion resistance of NAB with different degrees of corrosion. According to the results presented in Fig. 14, the cavitation erosion resistance of the NAB in ASW could be confidently estimated within 60 days.

This work showed that the cavitation erosion performance of the ASW- and the BASW-immersed NAB samples were different (Fig. 13), and possible failure mechanisms were concluded in a schematic diagram (Fig. 15). The increased volume loss due to the extended immersion time in ASW/BASW was much lower for the BASW-immersed samples. As the only variable was the existence of the biofilm by *Bacillus* sp. in this work, it is sensible to ascribe the phenomenon to the effect of the biofilm. The presence of the biofilm delayed the corrosion process of the NAB in ASW via inhibiting the dissolution of Cu and Al from the surface of NAB. The delayed corrosion process of the BASW-immersed NAB resulted in very

limited detachment of hard κ phases from the surface (Fig. 7d2, Fig. 15bII), while the κ phases in the ASW-immersed NAB were almost removed (Fig. 7d1, Fig. 15aII). The direct outcome of the difference in the amount of the remaining κ phases was the change of the Vickers hardness Fig. 12, which was strongly correlated to the cavitation erosion performance (Fig. 14). Meanwhile, according to the *in-situ* observation of the NAB exposed to cavitation erosion (Fig. 4), κ phases play a dominant role in resisting cavitation erosion, where the detachment of the κ phases leaves the α phase matrix unprotected, subsequently causing severe erosion (Fig. 15aIII). To summarise, the existence of the biofilm by *Bacillus* sp. on the NAB kept the κ phases almost intact via delaying the corrosion process in ASW immersion, which contributed to the less compromised cavitation erosion resistance of the BASW-immersed NAB compared to the ASW-immersed NAB (Fig. 15bIII).

However, the fouling microorganism *Bacillus* sp. only exhibits a significant MICI effect on the adhesion to NAB, while there are other microorganisms showing the MIC effect [9–13], which can have a significant impact on cavitation erosion-corrosion due to the accelerated corrosion rate. Thus, it is worthwhile to investigate how the fouling microorganisms with MIC effect influence the cavitation erosion-corrosion of materials. Furthermore, the bioadhesion of bacteria and small microorganisms is the initial stage of fouling, and large microorganisms (such as barnacles and bryozoans) will be adhered subsequently [59,60]. From the perspective of the current research and application status, it is imperative to develop a material with good cavitation resistance and antifouling capabilities.

4. Conclusions

This study investigated the influence of the *Bacillus* sp. adhesion on cavitation erosion performance of NAB. The conclusions are summarized as follows:

- (1) The κ phases played a dominant role in resisting cavitation erosion. The detachment of κ phases can cause severe material loss from the exposed α phase matrix during cavitation erosion.
- (2) *Bacillus* sp. biofilm could significantly reduce the corrosion process of NAB in ASW and keep κ phases almost intact, which was crucial to resist cavitation erosion. Without the protection of the biofilm, κ phases were almost removed from the NAB in ASW immersion, resulting in significantly compromised cavitation erosion resistance.
- (3) A confident relationship between increased mass loss and the decreased hardness for the ASW/BASW-immersed NAB samples subjected to cavitation erosion was raised.

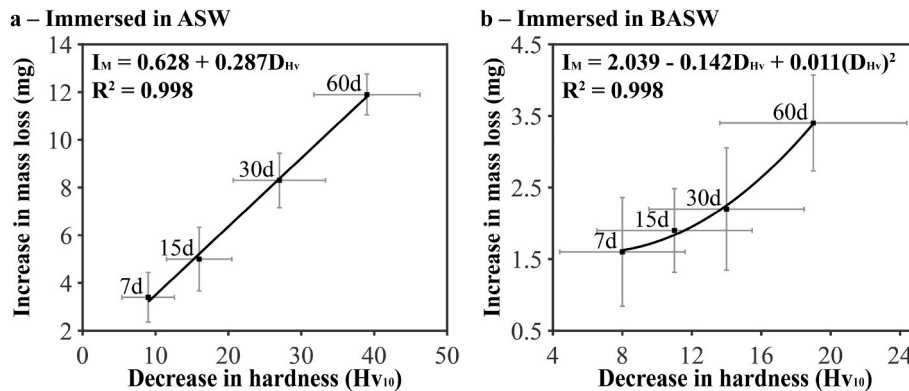


Fig. 14. Plots of increased mass loss (I_m) vs. decreased hardness (D_{Hv}) for the ASW/BASW-immersed NAB samples subjected to cavitation erosion for 6 h a, immersion in ASW; b, immersion in BASW.

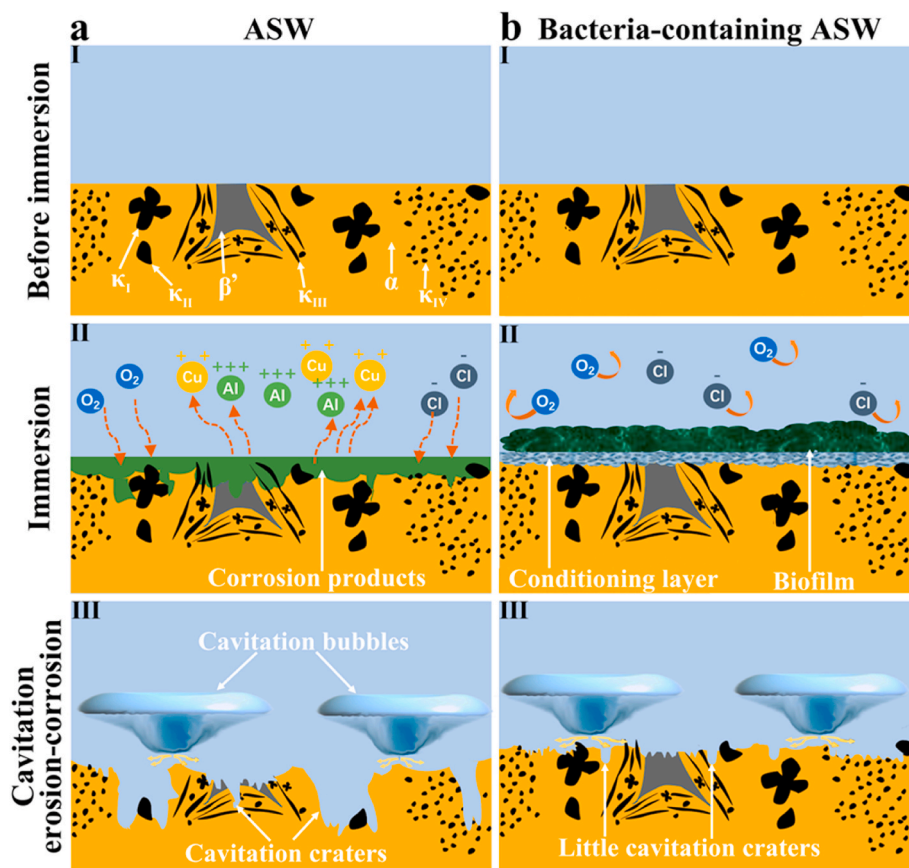


Fig. 15. Schematics demonstrating possible failure mechanisms of the ASW/BASW-immersed NAB samples subjected to cavitation erosion. a, immersion in ASW; b, immersion in BASW.

Author statement

I declare that this work has not been published nor is being submitted simultaneously elsewhere. The authors declare no competing interests. All authors have checked the manuscript and agreed to its submission. I take full responsibility for its submission.

Declaration of competing interest

The authors declare that they have no known competing financial interests or personal relationships that could have appeared to influence the work reported in this paper.

Acknowledgements

This work was supported by the Zhejiang Provincial Natural Science Foundation of China (grant # LZ22E090001), Ningbo 3315 Talents Program (grant # 2020A-29-G), and Chinese Academy of Sciences President's International Fellowship Initiative (grant # 2020VEA0005).

References

- [1] R.J.K. Wood, Marine wear and tribocorrosion, *Wear* 376 (2017) 893–910, <https://doi.org/10.1016/j.wear.2017.01.076>.
- [2] Z.B. Zheng, J. Long, S. Wang, H. Li, J. Wang, K.H. Zheng, Cavitation erosion-corrosion behaviour of Fe-10Cr martensitic steel microalloyed with Zr in 3.5 % NaCl solution, *Corrosion Sci.* 184 (2021) 109382, <https://doi.org/10.1016/j.corsci.2021.109382>.
- [3] R. Pecha, B. Gompf, Microimplosions: cavitation collapse and shock wave emission on a nanosecond time scale, *Phys. Rev. Lett.* 84 (2000) 1328–1330, <https://doi.org/10.1103/PhysRevLett.84.1328>.
- [4] L. Ye, X. Zhu, Y. He, X. Wei, Ultrasonic cavitation damage characteristics of materials and a prediction model of cavitation impact load based on size effect, *Ultrason. Sonochem.* 66 (2020) 105115, <https://doi.org/10.1016/j.ultrasonch.2020.105115>.
- [5] H.J. Zhang, Y.F. Gong, X.Y. Chen, A. McDonald, H. Li, A comparative study of cavitation erosion resistance of several HVOF-sprayed coatings in deionized water and artificial seawater, *J. Therm. Spray Technol.* 28 (2019) 1060–1071, <https://doi.org/10.1007/s11666-019-00869-x>.
- [6] S.K. Yan, G.L. Song, Z.X. Li, H.N. Wang, D.J. Zheng, F.Y. Cao, M. Horynova, M. S. Dargusch, L. Zhou, A state-of-the-art review on passivation and biofouling of Ti and its alloys in marine environments, *J. Mater. Sci. Technol.* 34 (2018) 421–435, <https://doi.org/10.1016/j.jmst.2017.11.021>.
- [7] X.X. Sheng, Y.P. Ting, S.A. Pehkonen, The influence of sulphate-reducing bacteria biofilm on the corrosion of stainless steel AISI 316, *Corrosion Sci.* 49 (2007) 2159–2176, <https://doi.org/10.1016/j.corsci.2006.10.040>.
- [8] D.K. Xu, Y.C. Li, F.M. Song, T.Y. Gu, Laboratory investigation of microbiologically influenced corrosion of C1018 carbon steel by nitrate reducing bacterium *Bacillus licheniformis*, *Corrosion Sci.* 77 (2013) 385–390, <https://doi.org/10.1016/j.corsci.2013.07.044>.
- [9] F.L. Liu, J. Zhang, C.X. Sun, Z.H. Yu, B.R. Hou, The corrosion of two aluminium sacrificial anode alloys in SRB-containing sea mud, *Corrosion Sci.* 83 (2014) 375–381, <https://doi.org/10.1016/j.corsci.2014.03.003>.
- [10] H.W. Liu, C.Y. Fu, T.Y. Gu, G.A. Zhang, Y.L. Lv, H.T. Wang, H.F. Liu, Corrosion behavior of carbon steel in the presence of sulfate reducing bacteria and iron oxidizing bacteria cultured in oilfield produced water, *Corrosion Sci.* 100 (2015) 484–495, <https://doi.org/10.1016/j.corsci.2015.08.023>.
- [11] P.Y. Zhang, D.K. Xu, Y.C. Li, K. Yang, T.Y. Gu, Electron mediators accelerate the microbiologically influenced corrosion of 304 stainless steel by the *Desulfovibrio vulgaris* biofilm, *Bioelectrochemistry* 101 (2015) 14–21, <https://doi.org/10.1016/j.bioelechem.2014.06.010>.
- [12] R. Jia, D.Q. Yang, D.K. Xu, T.Y. Gu, Electron transfer mediators accelerated the microbiologically influence corrosion against carbon steel by nitrate reducing *Pseudomonas aeruginosa* biofilm, *Bioelectrochemistry* 118 (2017) 38–46, <https://doi.org/10.1016/j.bioelechem.2017.06.013>.
- [13] Y.C. Li, S.Q. Feng, H.M. Liu, X.K. Tian, Y.Y. Xia, M. Li, K. Xu, H.B. Yu, Q.P. Liu, C. F. Chen, Bacterial distribution in SRB biofilm affects MIC pitting of carbon steel studied using FIB-SEM, *Corrosion Sci.* 167 (2020) 10, <https://doi.org/10.1016/j.corsci.2020.108512>.
- [14] S.L. Li, L. Li, Q. Qu, Y.X. Kang, B.L. Zhu, D.T. Yu, R. Huang, Extracellular electron transfer of *Bacillus cereus* biofilm and its effect on the corrosion behaviour of 316L stainless steel, *Colloids Surf., B* 173 (2019) 139–147, <https://doi.org/10.1016/j.colsurfb.2018.09.059>.

- [15] B.D. Mert, M.E. Mert, G. Kardas, B. Yazici, The role of *Spirulina platensis* on corrosion behavior of carbon steel, *Mater. Chem. Phys.* 130 (2011) 697–701, <https://doi.org/10.1016/j.matchemphys.2011.07.051>.
- [16] F.M. AlAbbas, S.M. Bholra, J.R. Spear, D.L. Olson, B. Mishra, The shielding effect of wild type iron reducing bacterial flora on the corrosion of linepipe steel, *Eng. Fail. Anal.* 33 (2013) 222–235, <https://doi.org/10.1016/j.engfailanal.2013.05.020>.
- [17] R. Zuo, Biofilms: strategies for metal corrosion inhibition employing microorganisms, *Appl. Microbiol. Biotechnol.* 76 (2007) 1245–1253, <https://doi.org/10.1007/s00253-007-1130-6>.
- [18] N. Aimeur, K. Houali, L. Hamadou, N. Benbrahim, A. Kadri, Influence of strain *Bacillus cereus* bacterium on corrosion behaviour of carbon steel in natural sea water, *Corrosion Eng. Sci. Technol.* 50 (2015) 579–588, <https://doi.org/10.1179/1743278215y.0000000022>.
- [19] A. Nagiub, F. Mansfeld, Evaluation of microbiologically influenced corrosion inhibition (MICI) with EIS and ENA, *Electrochim. Acta* 47 (2002) 2319–2333, [https://doi.org/10.1016/s0013-4686\(02\)00082-8](https://doi.org/10.1016/s0013-4686(02)00082-8).
- [20] Q.N. Song, Y. Tong, N. Xu, S.Y. Sun, H.L. Li, Y.F. Bao, Y.F. Jiang, Z.B. Wang, Y. X. Qiao, Synergistic effect between cavitation erosion and corrosion for various copper alloys in sulphide-containing 3.5% NaCl solutions, *Wear* 450 (2020) 203258, <https://doi.org/10.1016/j.wear.2020.203258>.
- [21] L.M. Zhang, A.L. Ma, H. Yu, A.J. Umoh, Y.G. Zheng, Correlation of microstructure with cavitation erosion behaviour of a nickel-aluminum bronze in simulated seawater, *Tribol. Int.* 136 (2019) 250–258, <https://doi.org/10.1016/j.triboint.2019.03.071>.
- [22] Z.B. Qin, Q. Zhang, Q. Luo, Z. Wu, B. Shen, L. Liu, W.B. Hu, Microstructure design to improve the corrosion and cavitation corrosion resistance of a nickel-aluminum, *Corrosion Sci.* 139 (2018) 255–266, <https://doi.org/10.1016/j.corsci.2018.04.043>.
- [23] J. Basumatary, M. Nie, R.J.K. Wood, The synergistic effects of cavitation erosion–corrosion in ship propeller materials, *J. Bio- Tribo-Corros.* 1 (2015) 12, <https://doi.org/10.1007/s40735-015-0012-1>.
- [24] J. Basumatary, R.J.K. Wood, Synergistic effects of cavitation erosion and corrosion for nickel aluminium bronze with oxide film in 3.5% NaCl solution, *Wear* 376 (2017) 1286–1297, <https://doi.org/10.1016/j.wear.2017.01.047>.
- [25] J. Basumatary, R.J.K. Wood, Different methods of measuring synergy between cavitation erosion and corrosion for nickel aluminium bronze in 3.5% NaCl solution, *Tribol. Int.* 147 (2020) 12, <https://doi.org/10.1016/j.triboint.2017.08.006>.
- [26] Z. Wu, Y.F. Cheng, L. Liu, W.J. Lv, W.B. Hu, Effect of heat treatment on microstructure evolution and erosion-corrosion behavior of a nickel-aluminum bronze alloy in chloride solution, *Corrosion Sci.* 98 (2015) 260–270, <https://doi.org/10.1016/j.corsci.2015.05.037>.
- [27] ASTM D1141-98, *Standard Practice for the Preparation of Substitute Ocean Water*, ASTM International, West Conshohocken, Pennsylvania, United States, 2013.
- [28] L. Abdoli, X.K. Suo, H. Li, Distinctive colonization of *Bacillus sp* bacteria and the influence of the bacterial biofilm on electrochemical behaviors of aluminum coatings, *Colloids Surf., B* 145 (2016) 688–694, <https://doi.org/10.1016/j.colsurfb.2016.05.075>.
- [29] ASTM G32-16(2021)e1, *Standard Test Method for Cavitation Erosion Using Vibratory Apparatus*, ASTM International, West Conshohocken, Pennsylvania, United States, 2021.
- [30] Y. Tian, H. Zhao, R. Yang, X. Liu, X. Chen, J. Qin, A. McDonald, H. Li, *In-situ* SEM investigation on stress-induced microstructure evolution of austenitic stainless steels subjected to cavitation erosion and cavitation erosion-corrosion, *Mater. Des.* 213 (2022) 110314, <https://doi.org/10.1016/j.matdes.2021.110314>.
- [31] J.A. Wharton, R.C. Barik, G. Kear, R.J.K. Wood, K.R. Stokes, F.C. Walsh, The corrosion of nickel-aluminum bronze in seawater, *Corrosion Sci.* 47 (2005) 3336–3367, <https://doi.org/10.1016/j.corsci.2005.05.053>.
- [32] M.E. Moussa, M.A. Waly, M. Amin, Effect of high intensity ultrasonic treatment on microstructural modification and hardness of a nickel-aluminum bronze alloy, *J. Alloys Compd.* 741 (2018) 804–813, <https://doi.org/10.1016/j.jallcom.2018.01.218>.
- [33] B.B. Zhang, J.Z. Wang, F.Y. Yan, Load-dependent tribocorrosion behaviour of nickel-aluminum bronze in artificial seawater, *Corrosion Sci.* 131 (2018) 252–263, <https://doi.org/10.1016/j.corsci.2017.11.028>.
- [34] Y. Ding, Y.T. Lv, B.J. Zhao, Y.F. Han, L.Q. Wang, W.J. Lu, Response relationship between loading condition and corrosion fatigue behavior of nickel-aluminum bronze alloy and its crack tip damage mechanism, *Mater. Char.* 144 (2018) 356–367, <https://doi.org/10.1016/j.matchar.2018.07.033>.
- [35] S.S.M. Tavares, N.M. Mota, H.R. da Igreja, C. Barbosa, J.M. Pardal, Microstructure, mechanical properties, and brittle fracture of a cast nickel-aluminum-bronze (NAB) UNS C95800, *Eng. Fail. Anal.* 128 (2021) 105606, <https://doi.org/10.1016/j.engfailanal.2021.105606>.
- [36] M. Moradi, Z.L. Song, X. Tao, Introducing a novel bacterium, *Vibrio neoaledonicus sp.*, with the highest corrosion inhibition efficiency, *Electrochem. Commun.* 51 (2015) 64–68, <https://doi.org/10.1016/j.elecom.2014.12.007>.
- [37] Z. Filip, S. Hermann, An attempt to differentiate *Pseudomonas spp.* and other soil bacteria by FT-IR spectroscopy, *Eur. J. Soil Biol.* 37 (2001) 137–143, [https://doi.org/10.1016/s1164-5563\(01\)01078-0](https://doi.org/10.1016/s1164-5563(01)01078-0).
- [38] G.Y. Long, P.T. Zhu, Y. Shen, M.P. Tong, Influence of extracellular polymeric substances (EPS) on deposition kinetics of bacteria, *Environ. Sci. Technol.* 43 (2009) 2308–2314, <https://doi.org/10.1021/es802464v>.
- [39] Q.N. Song, Y.G. Zheng, D.R. Ni, Z.Y. Ma, Studies of the nobility of phases using scanning Kelvin probe microscopy and its relationship to corrosion behaviour of Ni-Al bronze in chloride media, *Corrosion Sci.* 92 (2015) 95–103, <https://doi.org/10.1016/j.corsci.2014.11.039>.
- [40] Z.B. Qin, D.H. Xia, Y.W. Zhang, Z. Wu, L. Liu, Y.T. Lv, Y.C. Liu, W.B. Hu, Microstructure modification and improving corrosion resistance of laser surface quenched nickel-aluminum bronze alloy, *Corrosion Sci.* 174 (2020) 10, <https://doi.org/10.1016/j.corsci.2020.108744>.
- [41] R. Babic, M. Metikos-Hukovic, M. Loncar, Impedance and photoelectrochemical study of surface layers on Cu and Cu-10Ni in acetate solution containing benzotriazole, *Electrochim. Acta* 44 (1999) 2413–2421, [https://doi.org/10.1016/s0013-4686\(98\)00367-3](https://doi.org/10.1016/s0013-4686(98)00367-3).
- [42] B. Sabbaghzadeh, R. Parvizi, A. Davoodi, M.H. Moayed, Corrosion evaluation of multi-pass welded nickel-aluminum bronze alloy in 3.5% sodium chloride solution: a restorative application of gas tungsten arc welding process, *Mater. Des.* 58 (2014) 346–356, <https://doi.org/10.1016/j.matdes.2014.02.019>.
- [43] Q.N. Song, Y.G. Zheng, D.R. Ni, Z.Y. Ma, Characterization of the corrosion product films formed on the as-cast and friction-stir processed Ni-Al bronze in a 3.5 wt% NaCl solution, *Corrosion* 71 (2015) 606–614, <https://doi.org/10.5006/1391>.
- [44] A. Schussler, H.E. Exner, The corrosion of nickel-aluminum bronzes in seawater. 1. Protective layer formation and the passivation mechanism, *Corrosion Sci.* 34 (1993) 1793–1802, [https://doi.org/10.1016/0010-938x\(93\)90017-b](https://doi.org/10.1016/0010-938x(93)90017-b).
- [45] B. Tribollet, J. Newman, Impedance model for a concentrated-solution: application to the electrodisolution of copper in chloride solutions, *J. Electrochem. Soc.* 131 (1984) 2780–2785, <https://doi.org/10.1149/1.2115407>.
- [46] O.E. Barcia, O.R. Mattos, N. Pebere, B. Tribollet, Mass-transport study for the electrodisolution of copper in 1M hydrochloric-acid solution by impedance, *J. Electrochem. Soc.* 140 (1993) 2825–2832, <https://doi.org/10.1149/1.2220917>.
- [47] S.A. Campbell, G.J.W. Radford, C.D.S. Tuck, B.D. Barker, Corrosion and galvanic compatibility studies of a high-strength copper-nickel alloy, *Corrosion* 58 (2002) 57–71, <https://doi.org/10.5006/1.3277305>.
- [48] M. Metikos-Hukovic, R. Babic, I.S. Roncevic, Z. Grubac, Corrosion behavior of the filmed copper surface in saline water under static and jet impingement conditions, *Corrosion* 68 (2012), 025002, <https://doi.org/10.5006/1.3683224>.
- [49] A.L. Ma, S.L. Jiang, Y.G. Zheng, W. Ke, Corrosion product film formed on the 90/10 copper-nickel tube in natural seawater: composition/structure and formation mechanism, *Corrosion Sci.* 91 (2015) 245–261, <https://doi.org/10.1016/j.corsci.2014.11.028>.
- [50] D. Nakhaie, A. Davoodi, A. Imani, The role of constituent phases on corrosion initiation of NiAl bronze in acidic media studied by SEM-EDS, AFM and SKPFM, *Corrosion Sci.* 80 (2014) 104–110, <https://doi.org/10.1016/j.corsci.2013.11.017>.
- [51] F.F. Yang, H.J. Kang, E.Y. Guo, R.G. Li, Z.N. Chen, Y.H. Zeng, T.M. Wang, The role of nickel in mechanical performance and corrosion behaviour of nickel-aluminum bronze in 3.5 wt.% NaCl solution, *Corrosion Sci.* 139 (2018) 333–345, <https://doi.org/10.1016/j.corsci.2018.05.012>.
- [52] H. Wang, J.H. Xu, X.S. Du, H.B. Wang, X. Cheng, Z.L. Du, Stretchable and self-healing polyurethane coating with synergistic anticorrosion effect for the corrosion protection of stainless steels, *Prog. Org. Coating* 164 (2022) 8, <https://doi.org/10.1016/j.porgcoat.2021.106672>.
- [53] J. Yang, Z.B. Wang, Y.X. Qiao, Y.G. Zheng, Synergistic effects of deposits and sulfate reducing bacteria on the corrosion of carbon steel, *Corrosion Sci.* 199 (2022) 110210, <https://doi.org/10.1016/j.corsci.2022.110210>.
- [54] Y.H. Zeng, F.F. Yang, Z.N. Chen, E.Y. Guo, M.Q. Gao, X.J. Wang, H.J. Kang, T. M. Wang, Enhancing mechanical properties and corrosion resistance of nickel-aluminum bronze via hot rolling process, *J. Mater. Sci. Technol.* 61 (2021) 186–196, <https://doi.org/10.1016/j.jmst.2020.05.024>.
- [55] S. Hong, Y.P. Wu, J.F. Zhang, Y.G. Zheng, Y.J. Qin, W.W. Gao, G.Y. Li, Cavitation erosion behavior and mechanism of HVOF sprayed WC-10Co-4Cr coating in 3.5 wt % NaCl solution, *Trans. Indian Inst. Met.* 68 (2015) 151–159, <https://doi.org/10.1007/s12666-014-0440-5>.
- [56] H.J. Zhang, X.Y. Chen, Y.F. Gong, Y. Tian, A. McDonald, H. Li, *In-situ* SEM observations of ultrasonic cavitation erosion behavior of HVOF-sprayed coatings, *Ultrason. Sonochem.* 60 (2020) 9, <https://doi.org/10.1016/j.ultsonch.2019.104760>.
- [57] J.K. Choi, A. Jayaprakash, G.L. Chahine, Scaling of cavitation erosion progression with cavitation intensity and cavitation source, *Wear* 278 (2012) 53–61, <https://doi.org/10.1016/j.wear.2012.01.008>.
- [58] S. Thapliyal, D.K. Dwivedi, On cavitation erosion behavior of friction stir processed surface of cast nickel aluminium bronze, *Wear* 376 (2017) 1030–1042, <https://doi.org/10.1016/j.wear.2017.01.030>.
- [59] M. Otani, T. Oumi, S. Uwai, T. Hanyuda, R.E. Prabowo, T. Yamaguchi, H. Kawai, Occurrence and diversity of barnacles on international ships visiting Osaka Bay, Japan, and the risk of their introduction, *Biofouling* 23 (2007) 277–286, <https://doi.org/10.1080/08927010701315089>.
- [60] S. Song, Y.K. Demirel, M. Atlar, Penalty of hull and propeller fouling on ship self-propulsion performance, *Appl. Ocean Res.* 94 (2020) 24, <https://doi.org/10.1016/j.apor.2019.102006>.